Discover Oncology

ANALYSIS Open Access

DLX2 marks an immunosuppressive dendritic-cell program that reshapes cytotoxic immunity and marks a tolerogenic microenvironment in lung adenocarcinoma

Heng Tian[1,2†], Hanyue Zhang[1†], Ran Wei[3†], Can Zhang[4†], Yuhan Liu[3†], Xinyi Wang[5], Bangjie Chen[6], Ziyue Fu[7*] and Feng Rong[1*]

[†]Heng Tian, Hanyue Zhang, Ran Wei, Can Zhang and Yuhan Liu have contributed equally to this work.

*Correspondence:
Ziyue Fu
2445011814@stu.ahmu.edu.cn
Feng Rong
wazhl1996@163.com
[1]Department of Radiation Oncology of Tumor Center, Lu'an Hospital Affiliated to Anhui Medical University, Lu'an, China
[2]Department of Oncology, The First Affiliated Hospital of Anhui Medical University, Hefei, China
[3]First Clinical Medical College, Anhui Medical University, Hefei, China
[4]Department of Orthopedics, Lu'an Hospital Affiliated to Anhui Medical University, Lu'an, China
[5]Department of Radiation Oncology, The First Affiliated Hospital of Anhui Medical University, Hefei, China
[6]Department of Oncology, Affiliated Drum Tower Hospital, Medical School of Nanjing University, Nanjing, China
[7]Department of Otorhinolaryngology, The First Affiliated Hospital of Anhui Medical University, Hefei, China

Abstract

Background The neuroactive ligand–receptor signaling pathway is increasingly recognized as a regulator of tumor–immune interactions, yet its contribution to lung adenocarcinoma (LUAD) progression and immune evasion remains poorly defined.

Methods We integrated multi-cohort transcriptomic datasets, including TCGA-LUAD, GTEx lung tissues, pan-cancer resources, single-cell RNA-seq spanning LUAD progression stages, dendritic-cell subtype analyses, pySCENIC regulon inference, ligand–receptor interaction modeling, and Visium spatial transcriptomics. Neuroactive ligand–associated genes were evaluated for tumor upregulation, prognostic relevance, pathway activity, immune-cell associations, transcriptional identity, cell–cell communication profiles, and spatial localization.

Results DLX2 emerged as the top neuroactive-associated candidate, showing robust tumor-specific upregulation and strong association with poor overall, progression-free, disease-specific, and disease-free survival in LUAD, with consistent adverse effects across multiple cancer types. DLX2 expression correlated with activation of cell-cycle, chromatin-remodeling and metabolic pathways, accompanied by a pronounced shift toward an immunosuppressive microenvironment characterized by enrichment of Tregs, exhausted T cells, and M2 macrophages and depletion of cytotoxic $CD8^+$ and NK cells. Single-cell profiling revealed that DLX2 is predominantly expressed in dendritic cells (DCs), where it defines a tolerogenic and hyper-activated DC state marked by NF-κB/TNF-driven exhaustion signatures and regulon activity dominated by ATF3, FOSL2, FOSB, and ZMIZ1. $DLX2^+$ DCs exhibited enhanced communication with Tregs and exhausted T cells through inhibitory ligand–receptor networks including CTLA4–CD80/CD86, PD-1–PD-L1, LGALS9–HAVCR2, and TGF-β pathways, while reducing interactions with effector lymphocytes. Spatial transcriptomics further demonstrated that $DLX2^+$ DCs are preferentially located within hypoxic, TGF-β–rich niches co-occupied by Tregs and Tex populations, indicating that $DLX2^+$ DCs serve as spatial and functional hubs of immune suppression.

Conclusions This study identifies DLX2 as a potential neuroimmune-associated driver of dendritic-cell–mediated immune tolerance in LUAD. DLX2 defines a dysfunctional DC phenotype that promotes T-cell exhaustion, macrophage polarization, and the formation of immunosuppressive tumor niches. These findings reveal a mechanistic link between neuroactive ligand signaling and immune evasion and highlight DLX2 as a promising biomarker and potential therapeutic target for reprogramming antitumor immunity in LUAD.

Keywords Neuroactive ligand–receptor signaling, Lung adenocarcinoma, DLX2, Single cell RNA seq

1 Introduction

Lung adenocarcinoma (LUAD) remains the leading cause of cancer mortality worldwide, and its clinical management continues to be challenged by profound intratumoral heterogeneity and widespread immune dysfunction [1–3]. Although immunotherapy has transformed the therapeutic landscape, only a subset of patients achieve durable responses, underscoring the need to elucidate the molecular programs that shape the immunosuppressive microenvironment characteristic of LUAD [4–7]. Increasing evidence indicates that tumor–immune interactions are influenced not only by classical oncogenic signaling but also by unexpected regulatory axes, including neuroimmune pathways traditionally associated with neuronal communication [8–10].

Among these pathways, neuroactive ligand–receptor signaling has recently attracted attention for its ability to modulate immune activation, cellular plasticity, and stress responses within non-neural tissues [9, 11]. Several studies have shown that neuropeptides, neurotransmitters, and their receptors are aberrantly expressed across malignancies and can support tumor growth, angiogenesis, and immune evasion [12, 13]. However, the extent to which neuroactive ligand–associated genes contribute to LUAD progression, particularly by reshaping the tumor immune microenvironment, remains largely unexplored. Identifying the neuroimmune components that endow tumors with immune-evasive properties may uncover novel regulatory hubs relevant to disease progression and immunotherapy outcomes.

Dendritic cells (DCs) are central architects of antitumor immunity, bridging innate and adaptive responses through antigen presentation and T-cell priming [14–16]. Yet within tumors, DCs frequently acquire dysfunctional or tolerogenic states characterized by impaired antigen presentation, heightened exhaustion signaling, and preferential support of regulatory T-cell expansion [17]. Such dysfunctional DC states are increasingly recognized as key drivers of T-cell exhaustion and immune escape in LUAD [18]. Despite these advances, the transcriptional cues that determine whether DCs adopt immunostimulatory or immunosuppressive phenotypes in the tumor context remain incompletely defined. Whether neuroimmune-related genes regulate DC identity and function has not been systematically investigated.

In this context, our initial transcriptomic comparison between LUAD tumors and normal lung tissues revealed striking upregulation of neuroactive ligand–receptor pathways, suggesting the involvement of a neuroimmune axis in shaping tumor biology. Integrating neuroactive-ligand–associated gene sets with tumor-specific expression and prognostic markers led us to identify DLX2—a member of the distal-less homeobox family—as a compelling candidate. Although DLX2 has been implicated in developmental processes

and oncogenic programs in selected cancers, its role in immune regulation, dendritic-cell biology, or LUAD immunopathology is unknown.

Here, we comprehensively characterize the transcriptional, immunologic, and spatial landscape associated with DLX2 in LUAD across bulk, single-cell, and spatial transcriptomic modalities. We demonstrate that DLX2 defines a distinct tolerogenic dendritic-cell state that may establishes immunosuppressive niches, promotes T-cell exhaustion, and fosters macrophage polarization. These findings unveil a previously unrecognized neuroimmune regulatory mechanism in LUAD and position DLX2 as a central link between neuroactive signaling and tumor-driven immune tolerance.

2 Results

2.1 Neuroactive ligand–receptor signaling is prominently activated in LUAD and highlights DLX2 as a robust neuroimmune-associated risk gene

To investigate transcriptomic programs specifically activated in lung adenocarcinoma, we first compared TCGA-LUAD tumors with normal lung tissues from GTEx. KEGG enrichment analysis revealed that neuroactive ligand–receptor signaling was among the most significantly upregulated pathways in LUAD, surpassing canonical oncogenic pathways and indicating a strong neuroimmune component within the tumor transcriptome (Fig. 1A). To pinpoint neuroactive-associated drivers relevant to LUAD progression, we intersected neuroactive ligand–receptor genes curated by Dong et al. with genes upregulated in LUAD and those consistently associated with poor overall survival. This integrative filtering identified a focused set of 23 genes at the intersection of neuroactive signaling activation, tumor-specific elevation, and adverse prognosis (Fig. 1B). Random-forest modeling ranked these candidates by prognostic contribution, and DLX2 emerged as the most influential risk gene, far exceeding all other neuroactive-associated candidates (Fig. 1C). To further validate the robustness of the prognostic significance of DLX2, we performed a sensitivity analysis by stratifying patients into three groups based on DLX2 expression tertiles (Low, Medium, and High). Consistent with our primary median-based findings, the Kaplan-Meier analysis revealed a significant dose-dependent correlation between elevated DLX2 levels and unfavorable overall survival (Fig. 1D). Importantly, the prognostic impact of DLX2 extended well beyond LUAD: pan-cancer Cox and Kaplan–Meier analyses demonstrated consistent associations between DLX2 upregulation and poor outcomes across multiple malignancies (Fig. 1E–F). Supplemental analyses further established DLX2 as an adverse marker for progression-free survival (PFS), disease-free survival (DFS), and disease-specific survival (DSS), reinforcing its robustness across clinical endpoints and cancer types (Supplementary Figures S1–S3). Together, these results identify DLX2 as a neuroactive ligand–associated gene with strong and widespread prognostic relevance, positioning it as a compelling candidate for further mechanistic investigation in LUAD.

2.2 DLX2 is linked to proliferative and immunosuppressive transcriptional programs and associates with a dysfunctional immune microenvironment in LUAD

To define the biological programs underlying DLX2-associated risk, we examined pathway activity in TCGA-LUAD. DLX2 expression strongly correlated with activation of proliferative and chromatin-regulatory pathways, including cell-cycle progression, RNA splicing, ribosome biogenesis, nucleocytoplasmic transport, and ubiquitin-mediated

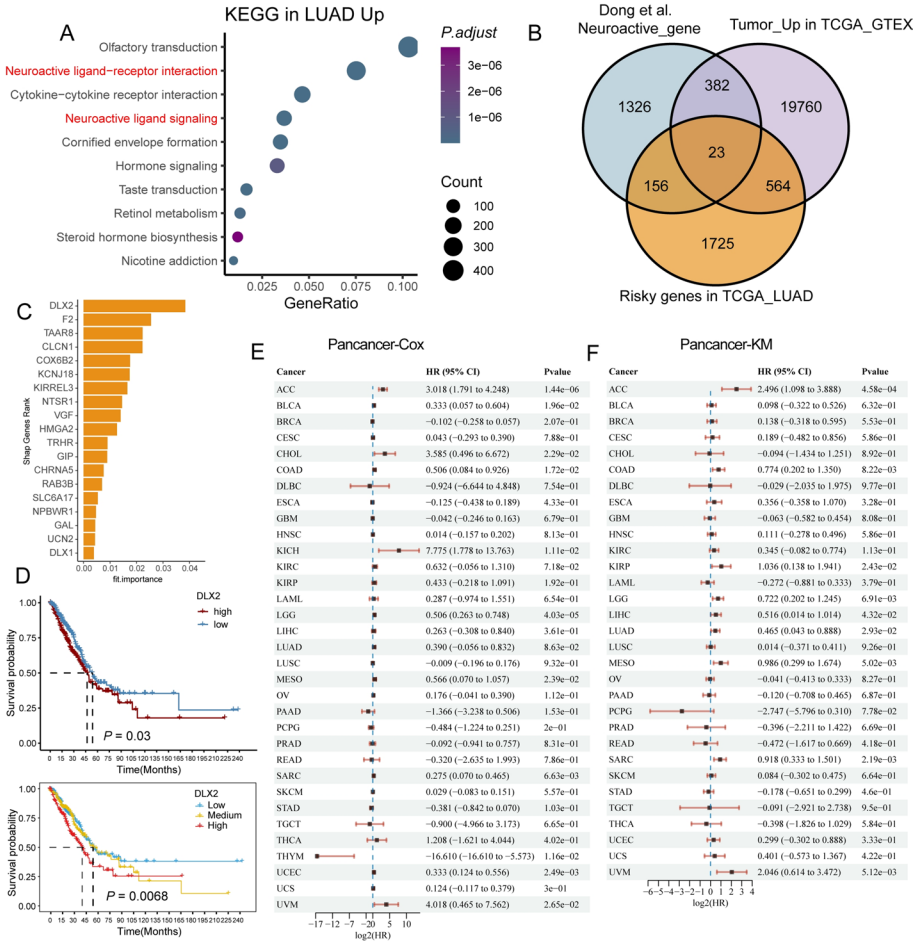

Fig. 1 Identification of DLX2 as a neuroactive-linked, tumor-upregulated, and prognostically adverse gene in LUAD. **A** Overlap between neuroactive ligand–receptor genes, LUAD-upregulated genes, and LUAD survival-associated genes, revealing DLX2 as a shared candidate. **B** Functional categorization of neuroactive ligand–receptor genes included in downstream screening. **C** Volcano plot identifying DLX2 as significantly upregulated in LUAD relative to normal lung tissues. **D** Kaplan–Meier survival curves showing that high DLX2 expression predicts worse OS; Patients were stratified into three groups (Low, Medium, and High) based on the tertiles of DLX2 expression to validate the robustness of the median-based survival analysis. **E** Pan-cancer hazard-ratio heatmap demonstrating the adverse prognostic effect of DLX2 across multiple TCGA tumor types. **F** Forest plot summarizing hazard ratios of neuroactive genes, highlighting DLX2 as a high-risk gene. **G** Random-forest variable-importance rankings identifying DLX2 as a key predictor of LUAD survival

proteolysis (Fig. 2A). Network-based enrichment further highlighted coordinated induction of ErbB signaling, xenobiotic metabolism, autophagy, and DNA replication modules (Fig. 2B), suggesting a broad remodeling of metabolic and transcriptional states that favor tumor growth. Consistent with this molecular profile, DLX2-high tumors exhibited increased stromal content, reduced immune infiltration, and higher ESTIMATE tumor purity (Fig. 2C), accompanied by elevated immune dysfunction scores across antigen-presentation, effector-cell, and cytokine-processing modules (Fig. 2D).

Given this strong immunologic signature, we next assessed DLX2 correlations with immune-cell populations across pan-cancer datasets. DLX2 was consistently associated with enriched regulatory T cells (Tregs), M2-polarized macrophages, neutrophils, and resting NK cells, whereas cytotoxic $CD8^+$ T cells, activated NK cells, and M1 macrophages showed negative associations (Fig. 2F). DLX2 was also positively correlated with myeloid-derived suppressor cell (MDSC) signatures and negatively correlated with

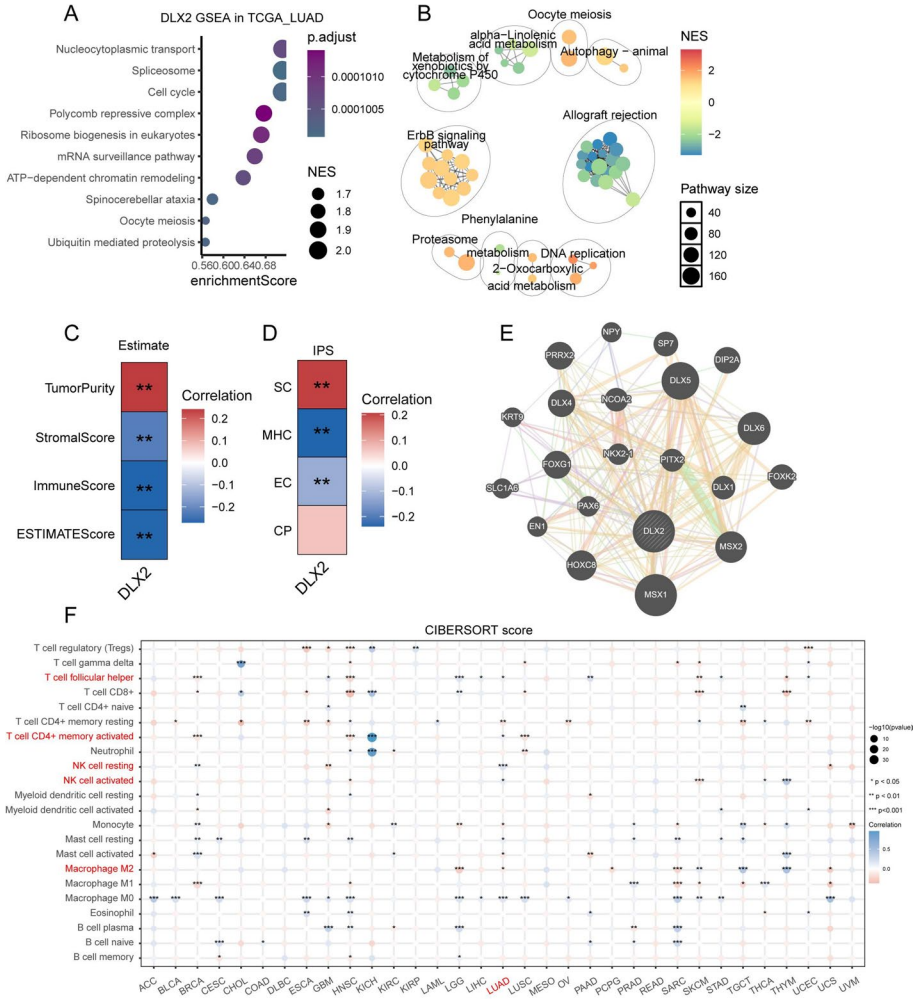

Fig. 2 DLX2 expression correlates with proliferative, metabolic, and immunosuppressive transcriptomic programs in LUAD. **A** Dot plot showing DLX2-associated pathway activation, including RNA metabolism, DNA replication, and signaling pathways. **B** KEGG network illustrating DLX2-linked functional clusters. **C** Immune, stromal, and tumor-purity scores stratified by DLX2 expression. **D** T-cell dysfunction and exhaustion scores associated with DLX2 levels. **E** PPI network positioning DLX2 within the HOX/MSX homeobox TF family. **F** Immune-cell correlation heatmap linking DLX2 to key immunosuppressive cell states

multiple cytotoxic T-cell states across multiple estimation frameworks, including xCell, CIBERSORT, TIMER, EPIC, and QUANTISEQ (Supplementary Figure S4). Integration of protein–protein interaction networks further supported a central regulatory role for DLX2, which clustered tightly with HOX, MSX, and DLX family transcription factors known to modulate developmental and immune-regulatory pathways (Fig. 2E).

Together, these results establish DLX2 as a key determinant of proliferative, metabolically active, and immunosuppressive tumor states, and implicate DLX2 expression in the emergence of T-cell dysfunction and myeloid-driven immune tolerance within the LUAD microenvironment.

2.3 DLX2 is predominantly expressed in dendritic cells and marks a transcriptionally exhausted, hyperactivated DC state that emerges during LUAD progression

To determine the cellular origin and context of DLX2 expression, we analyzed single-cell RNA-seq profiles spanning the histological continuum of LUAD (AIS–MIA–IAC).

UMAP embedding resolved major epithelial, immune, and stromal compartments (Fig. 3A; Supplementary Figure S5A), and annotation of early- to late-stage samples revealed progressive expansion of myeloid lineages, particularly dendritic cells (DCs), from AIS to invasive adenocarcinoma (Fig. 3B; Supplementary Figure S5B). Strikingly, DLX2 expression was sharply restricted to the myeloid compartment, with negligible expression in epithelial, fibroblast, endothelial, or lymphoid populations (Fig. 3C). Cell-type–specific marker analyses further supported this identity: genes such as LAMP3, CCR7, S100A9/12, C1QA/B/C, CLEC10A, and WDFY4 were enriched in DLX2^{+} DCs, consistent with the features of tolerogenic or regulatory DC populations implicated in T-cell exhaustion and immune suppression (Supplementary Figure S5C–D). Within

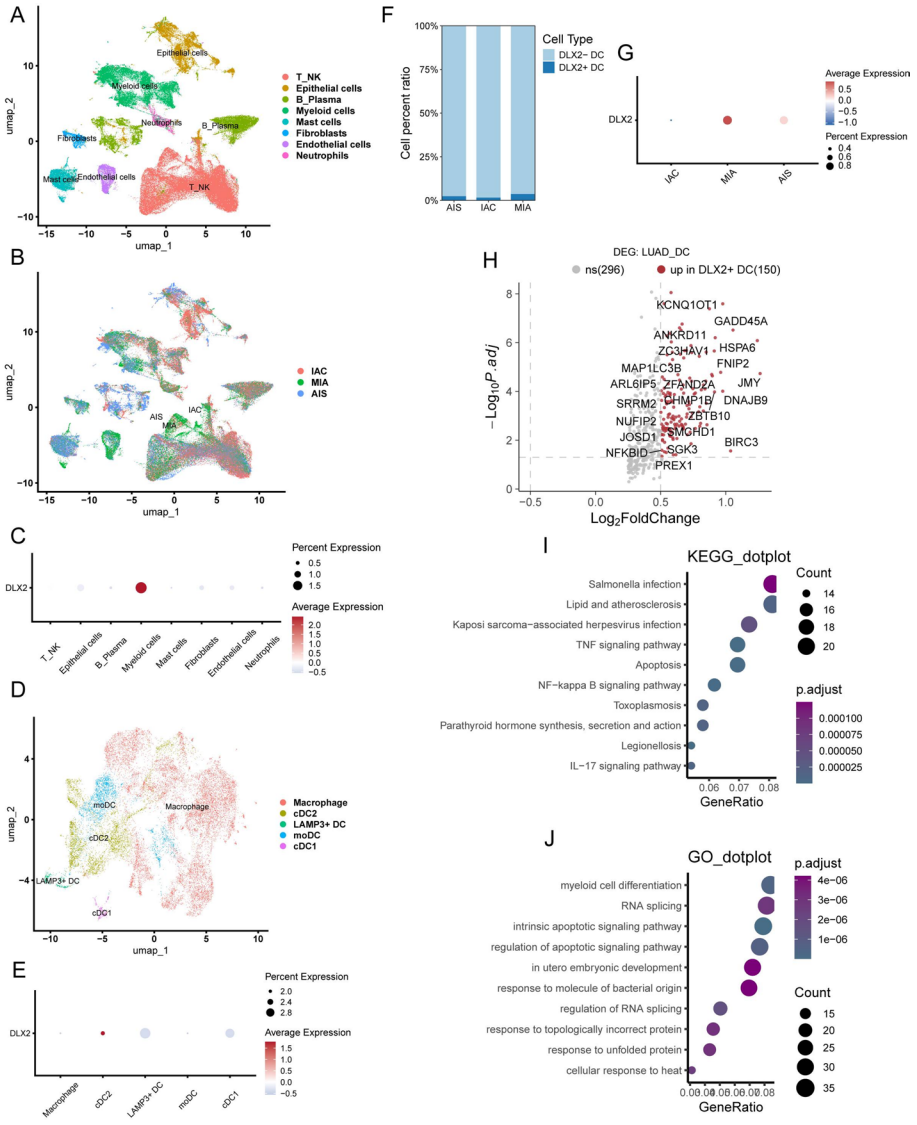

Fig. 3 Single-cell mapping identifies DLX2 as selectively expressed in dendritic-cell populations and enriched during LUAD progression. **A** UMAP of LUAD single-cell data showing major epithelial, immune, and stromal lineages (94542 cells; 9 patients). **B** Distribution of AIS, MIA, and IAC cells across the UMAP space. **C** DLX2 expression across major cellular compartments. **D** Identification of DC subsets including cDC1, cDC2, LAMP3^{+} DCs, and moDCs. **E** DLX2 expression concentrated within DC subpopulations. **F**, **G** Increased frequency and expression intensity of DLX2^{+} DCs across AIS-MIA-IAC progression. **H** Differentially expressed genes between DLX2^{+} and DLX2^{-} DCs. **I**, **J** KEGG and GO enrichment analyses showing stress-response and immunoregulatory programs in DLX2^{+} DCs

the myeloid lineage, DLX2 was almost exclusively confined to DC subsets—especially LAMP3^{+} regulatory DCs, monocyte-derived DCs, and cDC2 cells—while macrophages and cDC1 cells remained largely DLX2-negative (Fig. 3D–E). DLX2^{+} DCs increased markedly from AIS to IAC, suggesting that this program emerges alongside tumor progression (Fig. 3F–G).

Transcriptional profiling of DLX2^{+} versus DLX2^{-} DCs identified a robust set of upregulated genes involved in NF-κB activation, DNA damage responses, unfolded protein response, and cytokine signaling (Fig. 3H). Pathway enrichment confirmed strong activation of TNF/NF-κB signaling, apoptosis-related pathways, IL-17 and bacterial-stimulus responses, xenobiotic metabolism, and antigen-processing modules (Fig. 3I–J). These signatures collectively indicate a hyperactivated yet dysfunctional DC phenotype characterized by chronic inflammatory stimulation and immune-regulatory remodeling.

Together, these findings demonstrate that DLX2 is not a general tumor-cell marker but instead defines a specialized dendritic-cell state that becomes amplified during LUAD progression and is distinguished by a transcriptional program linked to chronic activation, antigen-processing imbalance, and immunosuppressive remodeling.

2.4 DLX2^{+} dendritic cells are governed by an immunosuppressive regulon program anchored by ATF3–FOSL2–FOSB–ZMIZ1 and reinforced by a cytokine-stress signaling axis

To delineate the transcriptional circuitry defining the dysfunctional phenotype of DLX2^{+} dendritic cells, we performed pySCENIC regulon analysis across DC subsets. DLX2^{+} DCs displayed a highly specific regulon profile dominated by ATF3, FOSL2, FOSB, FOS, and ZMIZ1—transcription factors known to orchestrate stress-induced tolerogenic reprogramming, restraint of antigen-presenting capacity, and promotion of dendritic-cell exhaustion (Fig. 4A). In contrast, DLX2^{-} DCs were enriched for IRF8, BCL3, JUND, CREM, and MAX regulons (Fig. 4B), representing canonical drivers of DC maturation, type-I interferon responses, and effective antigen presentation. This opposing regulon architecture indicates that DLX2 marks a transcriptional transition away from immunostimulatory conventional DC identity toward a regulatory/exhausted DC state.

Consistent with these regulon patterns, DLX2^{+} DCs exhibited markedly increased expression of multiple genes associated with immunoregulation, chronic activation, and antigen-processing imbalance (Fig. 4C). Integration with differential expression in Supplementary Fig. 6 further highlighted a coordinated cytokine-stress axis: DLX2^{+} DCs showed elevated TGFB1, STAT3, and XBP1, consistent with TGF-β–mediated immunosuppression, unfolded-protein-response activation, and tolerogenic DC maturation. Similarly, genes linked to DC dysfunction and NF-κB hyperactivation—including REL, RELB, BIRC3, and TNFSF9—were significantly upregulated in DLX2^{+} cells. Moreover, DLX2^{+} DCs expressed high levels of antigen-processing components such as B2M, CD74, HLA-A, and PSMB9, together with the migratory/tolerogenic marker CCR7, suggesting a paradoxical combination of enhanced antigen-processing machinery with impaired capacity to prime effective cytotoxic T-cell responses (Supplementary Figure S6A).

Network reconstruction confirmed that DLX2^{+} DCs assemble a dense immunoregulatory interaction module connecting ATF3, RELB, NF-κB components, co-inhibitory molecules, and MHC class-II pathways with broad downstream targets (Fig. 4D). This network links directly to mediators of T-cell exhaustion, apoptosis, IL-10/TGF-β

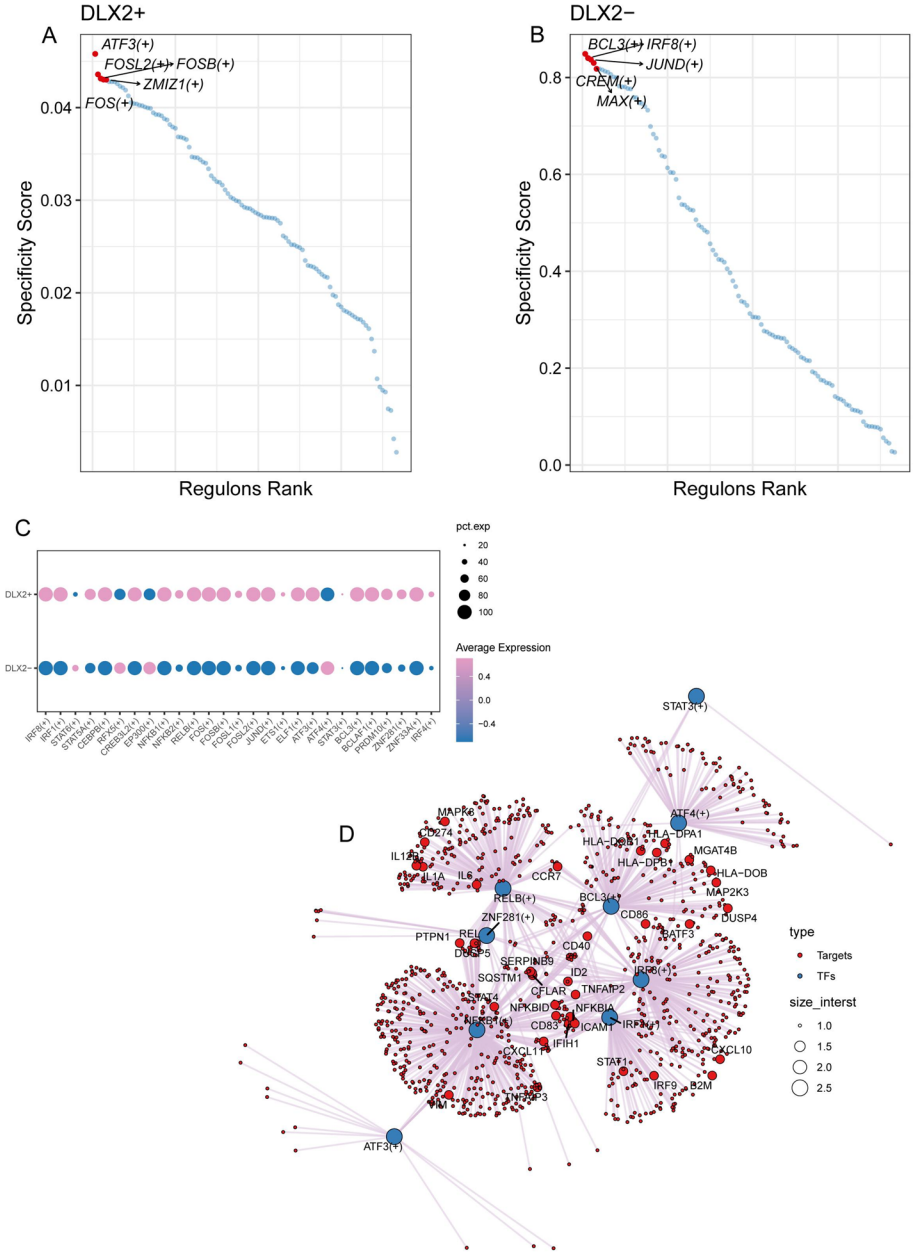

Fig. 4 SCENIC-based regulon analysis identifies an immunosuppressive ATF3–FOSL2–FOSB–ZMIZ1 transcriptional module defining DLX2^{+} DCs. **A** Regulon specificity scores highlighting top TF modules in DLX2^{+} DCs. **B** Regulon specificity in DLX2^{-} DCs dominated by IRF8- and JUND-centered modules. **C** Expression of selected transcription factors in DLX2^{+} vs. DLX2^{-} DCs. **D** SCENIC regulatory network illustrating TF-target architecture associated with DLX2^{+} DC function

signaling, and reduced lymphocyte recruitment. By contrast, DLX2^{-} DCs were associated with regulons that map to antigen cross-presentation, antiviral defense, and immunostimulatory states—consistent with their preserved functional identity.

Together, these results demonstrate that DLX2^{+} DCs are defined by a coherent transcriptional program combining ATF3–FOSL2–FOSB–ZMIZ1 regulon dominance with activation of TGF-β, NF-κB, UPR, and antigen-processing pathways. This integrated axis positions DLX2 as a central regulator of the shift from functional, IRF8-driven DCs to a hyperactivated yet immunosuppressive and exhaustion-prone DC state in LUAD.

2.5 DLX2$^+$ dendritic cells reshape the tumor immune landscape by expanding regulatory and exhausted T-cell populations, promoting M2 macrophage polarization, and engaging in extensive immunosuppressive ligand–receptor signaling

Given the potent immunoregulatory signature of DLX2$^+$ dendritic cells, we next examined how their abundance influences the broader immune-cell ecosystem. DLX2 expression varied widely across patient-derived DC samples (Fig. 5A), enabling stratification of tumors into DLX2-low and DLX2-high immune states. UMAP mapping revealed

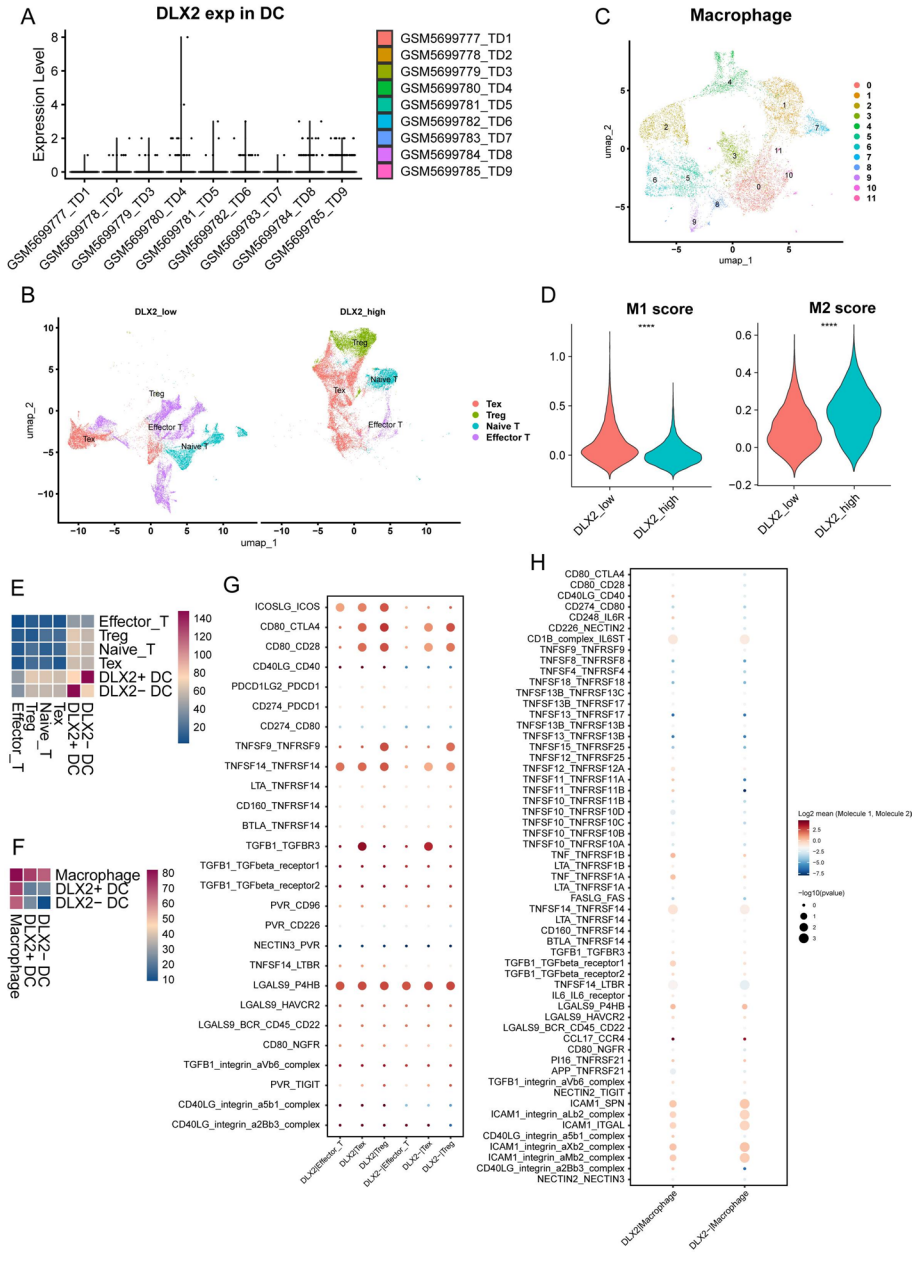

Fig. 5 DLX2$^+$ DCs is associated to T-cell dysfunction and M2 macrophage polarization through expanded inhibitory ligand–receptor interactions. **A** DLX2 expression levels across DC samples. **B** UMAP showing expansion of Tex and Tregs and reduction of naïve/effector T cells in DLX2-high tumors. **C** Macrophage states identified from scRNA-seq. **D** M1 and M2 polarization scores in DLX2-low vs. DLX2-high tumors. **E**, **F** Heatmaps displaying the correlation intensity between DLX2$^+$ DCs and immunosuppressive cell lineages. **G**, **H** Analysis of ligand–receptor predicted likelihood between DLX2$^+$ DCs and immunosuppressive cell lineages inferred via CellPhoneDB

that DLX2-high tumors exhibited a striking expansion of regulatory T cells (Tregs) and exhausted CD8⁺ T cells (Tex), accompanied by a reduction of naïve and effector T-cell subsets (Fig. 5B).

Integration of T-cell functional markers (Supplementary Fig. 7A) confirmed that DLX2-high tumors displayed high expression of exhaustion-associated genes—including PDCD1, TIGIT, LAYN, CTLA4, HAVCR2, and IKZF4—and reduced expression of cytotoxic mediators such as GZMA, GZMK, PRF1, and IFNG. Conversely, Treg markers including FOXP3, IL2RA, and CCR7 were markedly elevated. Population-level quantification further demonstrated that DLX2-high tumors are dominated by Tregs and Tex cells, whereas DLX2-low tumors retain higher proportions of naïve and effector T cells (Supplementary Fig. 7B). These patterns position DLX2⁺ DCs as potential upstream regulators of both T-cell exhaustion and regulatory T-cell expansion.

Macrophage analysis revealed a parallel shift in myeloid polarization: DLX2-high tumors exhibited a significant enrichment of M2 macrophages and depletion of M1 macrophages (Fig. 5C–D). This myeloid remodeling closely aligned with DLX2⁺ DC prevalence, as correlation matrices placed DLX2⁺ DCs together with Tregs, Tex cells, and M2 macrophages, whereas DLX2⁻ DCs clustered with effector T-cell states (Fig. 5E–F).

To uncover the mechanisms driving these shifts, we performed ligand–receptor modeling across DCs, T cells, and macrophages. DLX2⁺ DCs showed dominant engagement of inhibitory pathways with T cells, including robust CTLA4–CD80/CD86, PDCD1LG2–PDCD1, ICOSLG–ICOS, BTLA–TNFRSF14, LGALS9–HAVCR2, and multiple TNFSF–TNFRSF pairs (Fig. 5G). Notably, DLX2⁺ DCs exhibited increased TGF-β ligand expression and active TGF-β receptor interactions—consistent with their ability to induce Tregs and attenuate cytotoxic differentiation.

Interactions with macrophages revealed a complementary set of immunosuppressive communications: DLX2⁺ DCs engaged TGF-β/integrin complexes, LGALS9–HAVCR2, NECTIN–PVR networks, and CD40/CD40LG modules, collectively promoting anti-inflammatory M2 polarization (Fig. 5F). Broad ligand–receptor mapping demonstrated that DLX2⁺ DCs deploy a far more extensive inhibitory and co-regulatory communication repertoire than DLX2⁻ DCs, spanning TNF superfamily, integrin complexes, ICAM family, and TGF-β–related axes (Fig. 5H).

Together, these findings identify DLX2⁺ DCs as central architects of a multilayered immunosuppressive network in LUAD. By simultaneously promoting Treg expansion, driving CD8⁺ T-cell exhaustion, and fostering M2 macrophage polarization through extensive inhibitory ligand–receptor signaling, DLX2⁺ DCs actively sculpt a tumor microenvironment optimized for immune evasion and tumor progression.

2.6 Spatial transcriptomics reveals that DLX2⁺ dendritic cells localize within immunosuppressive niches enriched for Tregs, exhausted T cells, and M2-like macrophages, forming coordinated spatial hubs of immune tolerance

To determine whether the immunosuppressive programs associated with DLX2⁺ DCs translate into spatially organized niches within LUAD tissues, we integrated Visium spatial transcriptomics across multiple tumor sections (Fig. 6A). Spatial deconvolution revealed highly structured immune architectures: Tregs, Tex cells, macrophages, and DLX2⁺ DCs exhibited overlapping, compact regions of high abundance, whereas naïve and effector T cells were largely excluded from these areas (Fig. 6B). These findings

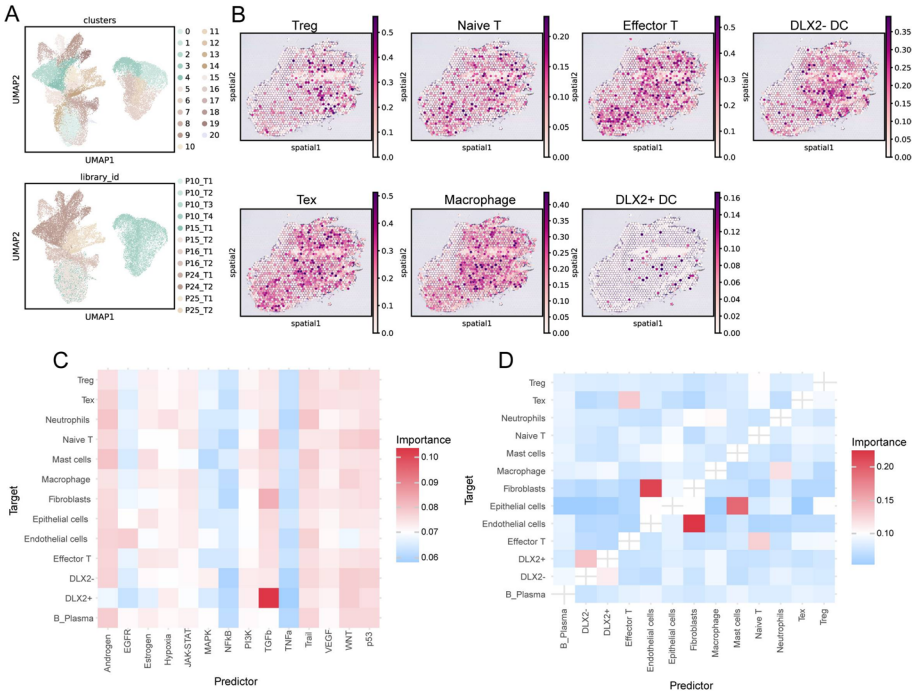

Fig. 6 Spatial transcriptomics reveals co-localized immunosuppressive niches centered on DLX2$^+$ dendritic cells. **A** UMAP of spatial transcriptomics libraries and cell clusters (29185 spots). **B** Spatial enrichment of Tregs, Tex, naïve T cells, effector T cells, macrophages, DLX2$^-$ DCs, and DLX2$^+$ DCs. **C** Pathway-to-cell influence matrix identifying TGF-β signaling as a major determinant of DLX2$^+$ DC spatial localization. **D** Cell–cell spatial influence matrix showing DLX2$^+$ DCs as predictors of Treg and Tex accumulation

indicate that DLX2$^+$ DCs do not distribute randomly but instead accumulate in microenvironments already enriched for immunosuppressive lymphoid and myeloid lineages.

To further interrogate the determinants of this spatial co-localization, we performed spatial-priority modeling to quantify the regulatory influence of signaling pathways and cell populations on one another. TGF-β signaling emerged as the strongest predictor of DLX2$^+$ DC localization (Fig. 6C), consistent with its known role in driving tolerogenic DC differentiation and Treg stability. Reciprocal modeling identified DLX2$^+$ DCs themselves as key predictors of Treg and Tex spatial enrichment, supporting a feed-forward circuit in which DLX2$^+$ DCs both arise within and reinforce immunosuppressive niches (Fig. 6D). Importantly, macrophage spatial dynamics mirrored this pattern: M2-associated macrophages strongly co-occurred with DLX2$^+$ DC–Treg–Tex regions, whereas M1-like inflammatory macrophages were depleted, mirroring the shifts observed in scRNA-seq analyses (Fig. 6B and D).

Taken together, these spatial data reveal that DLX2$^+$ DCs are not only transcriptionally distinct but also geographically positioned to function as organizational hubs of immune suppression. Their co-localization with Tregs, exhausted T cells, and M2-polarized macrophages defines a structurally coherent immunosuppressive ecosystem, indicating that DLX2$^+$ DCs shape LUAD progression by orchestrating both the molecular and spatial architecture of tumor-immune dysfunction.

3 Materials and methods

3.1 Data sources and preprocessing

Bulk RNA-seq data for lung adenocarcinoma (LUAD) were obtained from The Cancer Genome Atlas (TCGA-LUAD) and corresponding normal lung tissues from the Genotype-Tissue Expression (GTEx) project. To compare transcriptomic profiles between lung adenocarcinoma (LUAD) and normal tissues, gene expression data from the TCGA and GTEx cohorts were obtained from the UCSC Xena portal in a re-computed and harmonized format via the TOIL pipeline [19]. This standardization process significantly minimizes batch effects arising from different sequencing platforms and processing pipelines between the two databases. For all downstream differential expression and functional enrichment analyses, we utilized $\log_2$-transformed transcripts per million (TPM) values, which provide a more comparable metric across samples than raw counts. Gene expression matrices were downloaded as TPM values and $\log_2$-transformed after adding a pseudocount. Clinical information, including overall survival (OS), progression-free survival (PFS), disease-free survival (DFS), and disease-specific survival (DSS), was retrieved from UCSC Xena. Pan-cancer RNA-seq datasets spanning 33 tumor types were accessed through TCGA and uniformly processed for cross-cohort analyses. Neuroactive ligand–receptor genes were obtained from the published gene set by Dong et al. [20] (Supplementary Table S1).

3.2 Differential expression and pathway enrichment analyses

Differentially expressed genes (DEGs) between LUAD tumors and normal tissues were identified using DESeq2 with Benjamini–Hochberg correction. Gene set enrichment analysis (GSEA) was conducted with the clusterProfiler package [21] using KEGG, GO, and Hallmark gene sets. Enrichment significance was defined as false discovery rate (FDR) < 0.05. Pathway networks and functional clusters were visualized using enrichplot and igraph.

3.3 Prognostic modeling and random-forest ranking

To identify neuroactive-associated prognostic genes, we intersected: (1) neuroactive ligand–receptor genes, (2) LUAD tumor-upregulated genes, and (3) LUAD risk genes identified by univariate Cox regression. Candidate genes were ranked by random-forest models using survival randomForestSRC. Hazard ratios (HRs) were computed across TCGA pan-cancer cohorts using both Cox regression and Kaplan–Meier survival estimates. Candidate prognostic genes were prioritized using a Random Forest (RF) algorithm. To ensure the reproducibility of our model, the analysis was performed with a fixed seed of 1234, and the key hyperparameters were set as ntree = 1000 and mtry = 5. Prior to model training, genes were pre-filtered based on differential expression analysis ($|\log_2 FC| > 1$ and FDR < 0.05) and univariate Cox regression ($P < 0.05$).

3.4 Immune microenvironment estimation

Immune and stromal scores were calculated using ESTIMATE. Inferred immune cell fractions were obtained from CIBERSORT, xCell, EPIC, MCP-counter, TIMER, and TIDE. Immune dysfunction, T-cell exhaustion, Treg infiltration, and myeloid-derived suppressor cell (MDSC) signatures were scored from established gene sets. Correlation analyses used Spearman coefficients with FDR correction.

3.5 Single-cell RNA-seq analysis

scRNA-seq datasets covering the LUAD progression spectrum (AIS–MIA–IAC) were obtained from publicly available GEO datasets. Raw count matrices were processed using Seurat v4. Cells with >10% mitochondrial content or <200 detected genes were removed. Furthermore, DoubletFinder was employed to identify and remove potential doublets, ensuring that the downstream analysis was based on high-quality single cells. Normalization was performed by SCTransform with batch correction via Harmony. Clusters were annotated based on canonical markers for epithelial cells, T-cell subsets, B cells, macrophages, dendritic cells (cDC1, cDC2, LAMP3$^+$ DC, moDC), fibroblasts, endothelial cells, and mast cells. To specifically characterize the DLX2-expressing population, DLX2$^+$ DCs were defined as cells with a normalized count of DLX2 > 0 in the expression matrix. This binary classification allowed for a comparative analysis of transcriptional profiles between DLX2$^+$ and DLX2$^-$ dendritic cells.

3.6 Differential expression and functional profiling of DLX2$^+$ vs. DLX2$^-$ dendritic cells

DEGs between DLX2$^+$ and DLX2$^-$ DCs were identified using Wilcoxon rank-sum tests with Bonferroni correction. Pathway enrichment was performed with clusterProfiler for KEGG and GO terms. Stress-response, exhaustion, NF-κB, autophagy, unfolded protein response, and cytokine-signaling modules were quantified using AddModuleScore.

3.7 Regulon analysis using pySCENIC

Regulatory network inference for DLX2$^+$ and DLX2$^-$ DCs was performed using pySCENIC (v0.12.1). GRNBoost2 was used to infer co-expression modules; motif enrichment was conducted using cisTarget databases [22]; and regulon activity was scored using AUCell. Regulons were ranked by specificity index (RSS), and networks were visualized with Cytoscape.

3.8 Ligand–receptor interaction analysis

To investigate intercellular communication, we employed CellPhoneDB (v5.0), a publicly available repository of ligands, receptors, and their interactions. For the analysis, we utilized the normalized count data of single-cell clusters. An interaction was considered potentially active only if the corresponding ligand and receptor were expressed in at least 5% of cells in the respective clusters. To evaluate the statistical significance of the interactions, a permutation test ($n = 1000$) was performed, and interactions with $P < 0.05$ were prioritized for downstream visualization.

Cell-cell communication among DCs, T cells, and macrophages was inferred using CellPhoneDB. Inhibitory and co-stimulatory pathways—including CTLA4–CD80/CD86, PD-1/PD-L1, LGALS9–HAVCR2, BTLA–TNFRSF14, TGF-β ligand–receptor pairs, ICOS–ICOSLG, and TNFSF/TNFRSF families—were examined. Communication probability scores were computed from normalized expression of ligand–receptor pairs and significance assessed using permutation tests.

3.9 Macrophage polarization scoring

M1 and M2 macrophage states were quantified using validated gene signatures [23]. Scores were computed using Seurat's AddModuleScore and compared between DLX2-low and DLX2-high tumors. Macrophage clusters were annotated by expression of

canonical markers (CD68, C1QA/B/C, S100A8/A9, FCN1, IL1B for M1; MRC1, MSR1, CCR2, IL10, and APOE for M2).

3.10 Spatial transcriptomics analysis

Visium spatial transcriptomics data were processed and analyzed in Scanpy. Spatial deconvolution of immune and stromal cell populations was performed using cell2location. Co-localization patterns among DLX2$^+$ DCs, Tregs, Tex cells, macrophages, and stromal populations were examined using spatial correlation matrices and Moran's I statistics. Spatial-priority modeling was conducted using MistyR to quantify directional influences of signaling pathways—including TGF-β, NF-κB, JAK–STAT, and TNF signaling—on immune-cell localization.

3.11 Statistical analysis

Statistical analyses were performed using R. Two-group comparisons used Wilcoxon tests; multi-group comparisons used Kruskal–Wallis tests. Spearman correlations were used unless otherwise indicated. Multiple testing correction used FDR. To control the FDR in large-scale differential expression and pathway analyses, P-values were adjusted using the Benjamini–Hochberg procedure. For specific localized comparisons, the Bonferroni correction was applied where appropriate to maintain a stringent significance threshold. Survival significance was defined as $P < 0.05$.

4 Discussion

The present study reveals an unrecognized immunoregulatory axis in lung adenocarcinoma (LUAD) centered on a transcriptionally distinct dendritic-cell population marked by DLX2. Although dendritic cells (DCs) have long been regarded as pivotal orchestrators of antitumor immunity, accumulating evidence has indicated that tumor-conditioned DCs often acquire dysfunctional or tolerogenic features that suppress T-cell activation rather than promote it. Prior studies have highlighted LAMP3$^+$ DCs, moDCs, and migratory DC subsets as contributors to immune tolerance in solid tumors, yet the regulatory determinants that drive these dysfunctional phenotypes have remained incompletely defined. Our findings position DLX2 as a previously unappreciated molecular switch that marks and potentially drives a state of DC-mediated immune suppression, thereby extending and refining prevailing models of DC dysfunction in cancer.

Multiple studies have indicated that developmental transcription factors can be re-engaged by tumor-associated immune cells, leading to lineage plasticity or aberrant differentiation. Existing reports have emphasized TFs such as STAT3, IRF4, and ATF3 in reprogramming DC function within the tumor microenvironment [24, 25]. Our integrative regulon analysis reveals that DLX2$^+$ DCs are governed by an ATF3–FOSL2–FOSB–ZMIZ1 regulatory module enriched for stress-response, inflammatory, and unfolded-protein response programs—distinct from the IRF8-centered regulatory architecture typical of conventional cDC1 or cDC2 lineages [26]. This suggests that DLX2$^+$ DCs represent a transcriptionally rewired DC state rather than a canonical lineage subset. While previous work has linked ATF3 and AP-1 family TFs to tolerogenic or exhausted myeloid states [27], our study identifies DLX2 as a central node connecting these stress-activated regulons into a cohesive immunosuppressive identity,

thereby providing mechanistic insight into how LUAD microenvironments divert DC differentiation.

A notable contribution of this study is the demonstration of spatial organization of DLX2$^+$ DC–mediated immune suppression. Although recent spatial studies have shown that Tregs, exhausted CD8$^+$ T cells, and M2 macrophages tend to co-localize within immunosuppressive niches [28], the upstream initiators of these microarchitectures have remained unclear. Here, we show that DLX2$^+$ DCs consistently occupy the same spatial hubs as Tregs, Tex cells, and M2 macrophages across LUAD tissue sections. Furthermore, spatial-priority modeling indicates that TGF-β–rich microenvironments strongly predict the localization of DLX2$^+$ DCs, and reciprocally, that DLX2$^+$ DCs predict the spatial enrichment of Tregs and exhausted T cells. These findings complement prior studies demonstrating that TGF-β signaling shapes DC tolerogenicity and Treg stability, but they extend the concept by identifying DLX2$^+$ DCs as a structural organizer of immunosuppressive neighborhoods, rather than merely responding to them.

Importantly, our ligand–receptor analyses clarify how DLX2$^+$ DCs actively propagate immune dysfunction. Previous studies have shown that tumor-associated DCs can engage in PD-L1–PD-1 and CTLA4-CD80/CD86 interactions [29], but the breadth and intensity of inhibitory crosstalk has remained underappreciated. Our results reveal that DLX2$^+$ DCs deploy an expanded spectrum of inhibitory ligands—including TGF-β, LGALS9, PDCD1LG2, BTLA ligands, and multiple TNFSF/TNFRSF pairs—providing a multi-layered mechanism through which these cells suppress effector T-cell function, promote Treg differentiation, and reinforce M2 macrophage polarization. This suggests that DLX2$^+$ DCs may serve as an upstream "communication hub" that shapes the fate and function of multiple immune lineages simultaneously, filling a conceptual gap in our understanding of how tumor-driven immune suppression becomes systemically coordinated.

Our findings also have implications for immunotherapy. Immune checkpoint inhibitors (ICIs) rely on sufficient priming of tumor-specific T cells, a process heavily dependent on functional DCs [30, 31]. Multiple clinical studies have shown that dysfunctional or tolerogenic DC states correlate with diminished ICI responses in lung cancer [32, 33]. Given that DLX2$^+$ DCs are tightly associated with T-cell exhaustion, reduced effector T-cell infiltration, and M2 myeloid skewing, it is plausible that DLX2$^+$ DC abundance may serve as a biomarker of ICI resistance [31]. Moreover, given the extensive inhibitory signaling output of DLX2$^+$ DCs, targeting upstream drivers of this state—such as TGF-β signaling, ATF3/AP-1 activity, or metabolic stress pathways—may offer opportunities to re-sensitize tumors to immunotherapy. Several therapeutic candidates that modulate DC phenotype, including TGF-β inhibitors, AP-1 pathway modulators, and metabolic stress regulators, are already under clinical evaluation, suggesting that interventions aimed at the DLX2$^+$ DC program may be clinically actionable.

Despite its strengths, this study has limitations. While our multimodal analyses strongly suggest that DLX2 delineates a tolerogenic DC phenotype, direct lineage-tracing or functional perturbation experiments will be required to determine whether DLX2 is a potential driver or marker of this state. Additionally, although our data indicate that DLX2$^+$ DCs occupy immunosuppressive niches, the molecular cues that initiate DLX2 induction—whether derived from tumor cells, stromal components, or inflammatory stress—require further elucidation. Future experiments employing coculture

systems, organoids, or in vivo perturbations will be essential for establishing causality. Finally, given that similar DC states have been observed in other solid tumors, it will be important to investigate whether DLX2 marks a universal tolerogenic DC program or a LUAD-specific adaptation.

In summary, our work uncovers a previously unrecognized DLX2-defined dendritic-cell state that operates as a transcriptional, functional, and spatial organizer of immune suppression in LUAD. By integrating bulk, single-cell, ligand–receptor, and spatial transcriptomics, this study establishes $DLX2^+$ DCs as a central hub linking stress-response transcriptional programs to coordinated T-cell dysfunction and myeloid polarization. These findings fill a critical gap in our understanding of how tumor microenvironments establish immunosuppressive niches and suggest new avenues for therapeutic intervention aimed at reactivating antitumor immunity.

Supplementary Information

The online version contains supplementary material available at https://doi.org/10.1007/s12672-026-04692-z.

Supplementary Material 1. Supplementary Figure 1. Pan-cancer distribution and progression-free survival relevance of DLX2 expression. (A) DLX2 expression across tumor vs. normal tissues in the TCGA pan-cancer cohort, highlighting tumor types with significant up- or down-regulation. (B) Forest plot of progression-free survival (PFS) associations from Cox regression across cancers. (C) Kaplan–Meier–based hazard ratios showing pan-cancer PFS relevance of DLX2.

Supplementary Material 2. Supplementary Figure 2. Disease-free survival associations of DLX2 across the pan-cancer cohort. (A) Forest plot of DLX2 associations with disease-free survival (DFS) using Cox regression. (B) Kaplan–Meier–derived DFS hazard ratios across multiple cancer types.

Supplementary Material 3. Supplementary Figure 3. Disease-specific survival associations of DLX2 across the pan-cancer cohort. (A) Forest plot showing DLX2 hazard ratios for disease-specific survival (DSS) based on Cox regression. (B) Kaplan–Meier–derived DSS hazard ratios across cancer types.

Supplementary Material 4. Supplementary Figure 4. Correlation between DLX2 expression and immune infiltration signatures across pan-cancer datasets. (A) Heatmap showing partial correlations between DLX2 and various immune cell types—including $CD8^+$ T-cell subsets, Tregs, and MDSCs—across cancers using multiple immune-deconvolution algorithms (TIDE, xCell, QUANTISEQ, CIBERSORT, MCP-counter, EPIC, TIMER). Significant correlations are filled; non-significant values are cross-labeled.

Supplementary Material 5. Supplementary Figure 5. Cell-type annotation and composition of LUAD single-cell data across AIS, MIA, and IAC stages. (A) Dot plot showing canonical marker gene expression across major LUAD cell lineages (epithelial, fibroblasts, endothelial, mast cells, neutrophils, myeloid cells, plasma cells, T/NK cells). (B) Proportion of major cell types across AIS, MIA, and IAC stages. (C) Dot plot showing markers distinguishing macrophages, cDC1, cDC2, $LAMP3^+$ DCs, and moDCs. (D) UMAP showing DC subset distribution (cDC1, cDC2, moDC, $LAMP3^+$ DC).

Supplementary Material 6. Supplementary Figure 6. Key immunoregulatory, antigen-processing, and inflammatory genes significantly upregulated in $DLX2^+$ dendritic cells. (A) Violin plots comparing $DLX2^+$ vs. $DLX2^-$ DC expression of TGFB1, STAT3, BIRC3, REL, RELB, XBP1, TNFSF9, PSMB9, B2M, CD74, HLA-A, and CCR7.

Supplementary Material 7. Supplementary Figure 7. Functional T-cell signatures and population shifts associated with DLX2 expression. (A) Dot plot showing functional marker genes across T-cell subsets (Tex, Tregs, naïve T, effector T), including exhaustion markers (PDCD1, TIGIT, HAVCR2), cytotoxicity markers (GZMA, GZMK, PRF1, IFNG), and Treg markers (FOXP3, IL2RA). (B) Stacked bar plot showing the distribution of T-cell subsets between DLX2-low and DLX2-high tumors, highlighting increased Tex and Tregs in the DLX2-high group.

Supplementary Material 8.

Acknowledgements
Not applicable.

Author contributions
H.T. and R.W. conducted analysis and wrote the manuscript, H.Z., C.Z. and Y.L. created figures and tables and revised the manuscript, X.W. and B.C. searched for literature and revised the manuscript, Z.F. and F.R. designed the study, supervised the project, and revised the manuscript. B.C. provided financial support. All authors have reviewed and approved the manuscript.

Funding
This study is supported by Natural Science Research Major Project of Anhui Educational Committee (No.2023AH040077).

Data availability
Bulk RNA-seq data for lung adenocarcinoma were obtained from the TCGA-LUAD project through the UCSC Xena data portal (https://xenabrowser.net/). Expression matrices and corresponding clinical annotations were downloaded and harmonized for downstream differential, immunogenomic, and survival analyses. To characterize single-cell transcriptional heterogeneity within the LUAD tumor microenvironment, we integrated publicly available scRNA-seq datasets from GSE189357, which provide comprehensive profiling of epithelial, immune, and stromal lineages across LUAD specimens. Spatial transcriptomics validation was performed using the E-MTAB-13530 dataset, from which raw count matrices, spatial spot information, and metadata were retrieved and processed uniformly for cell-type deconvolution, spatial patterning, and microenvironmental interaction analyses. All secondary databases and computational resources used in the study have been explicitly included as follows. KEGG pathway annotations were obtained from the KEGG database (https://rest.kegg.jp/). Gene Ontology annotations were retrieved from the GO database (http://purl.obolibrary.org/obo/go.owl). MSigDB Hallmark gene sets were downloaded from MSigDB (https://www.gsea-msigdb.org/gsea/index.jsp). The Neuroactive ligand–receptor gene set from Dong et al. was accessed through the supplementary dataset (doi: 10.1093/bib/bbaf082). Immune-cell deconvolution was performed using CIBERSORT (https://cibersortx.stanford.edu/download.php), xCell (https://xcell.ucsf.edu/), EPIC (https://gfellerlab.shinyapps.io/EPIC_1-1/), MCP-counter (https://github.com/ebecht/MCPcounter), TIMER (https://cistrome.shinyapps.io/timer/) and TIDE (http://tide.dfci.harvard.edu/download/). Cell–cell communication analyses were carried out using CellPhoneDB (https://www.cellphonedb.org/downloads).

Declarations

Ethics approval and consent to participate
Not applicable.

Consent for publication
Not applicable.

Competing interests
The authors declare no competing interests.

Received: 19 December 2025 / Accepted: 16 February 2026
Published online: 27 February 2026

References

1. Barlesi F, Yao W, Duruisseaux M, Doucet L, Martínez AA, Gregorc V, et al. Adagrasib versus docetaxel in KRASG12C-mutated non-small-cell lung cancer (KRYSTAL-12): a randomised, open-label, phase 3 trial. Lancet. 2025;406(10503):615–26. https://doi.org/10.1016/S0140-6736(25)00866-9.
2. The L. Lung cancer treatment: 20 years of progress. Lancet. 2024;403(10445):2663. https://doi.org/10.1016/S0140-6736(24)01299-6.
3. Succony L, Rassl DM, Barker AP, McCaughan FM, Rintoul RC. Adenocarcinoma spectrum lesions of the lung: Detection, pathology and treatment strategies. Cancer Treat Rev. 2021;99:102237. https://doi.org/10.1016/j.ctrv.2021.102237.
4. Lahiri A, Maji A, Potdar PD, Singh N, Parikh P, Bisht B, et al. Lung cancer immunotherapy: progress, pitfalls, and promises. Mol Cancer. 2023;22(1):40. https://doi.org/10.1186/s12943-023-01740-y.
5. Liu S-YM, Zheng M-M, Pan Y, Liu S-Y, Li Y, Wu Y-L. Emerging evidence and treatment paradigm of non-small cell lung cancer. J Hematol Oncol. 2023;16(1):40. https://doi.org/10.1186/s13045-023-01436-2.
6. Skoulidis F, Goldberg ME, Greenawalt DM, Hellmann MD, Awad MM, Gainor JF, et al. STK11/LKB1 Mutations and PD-1 Inhibitor Resistance in KRAS-Mutant Lung Adenocarcinoma. Cancer Discov. 2018;8(7):822–35. https://doi.org/10.1158/2159-8290.CD-18-0099.
7. Wang J-B, Huang X, Li F-R. Impaired dendritic cell functions in lung cancer: a review of recent advances and future perspectives. Cancer Commun (Lond). 2019;39(1):43. https://doi.org/10.1186/s40880-019-0387-3.
8. Kalaora S, Nagler A, Wargo JA, Samuels Y. Mechanisms of immune activation and regulation: lessons from melanoma. Nat Rev Cancer. 2022;22(4):195–207. https://doi.org/10.1038/s41568-022-00442-9.
9. Amit M, Eichwald T, Roger A, Anderson J, Chang A, Vermeer PD, et al. Neuro-immune cross-talk in cancer. Nat Rev Cancer. 2025;25(8):573–89. https://doi.org/10.1038/s41568-025-00831-w.
10. Li G, Choi JE, Kryczek I, Sun Y, Liao P, Li S, et al. Intersection of immune and oncometabolic pathways drives cancer hyperprogression during immunotherapy. Cancer Cell. 2023. https://doi.org/10.1016/j.ccell.2022.12.008.
11. Ren L, Liu C, Çifcibaşı K, Ballmann M, Rammes G, Mota Reyes C, et al. Sensory neurons drive pancreatic cancer progression through glutamatergic neuron-cancer pseudo-synapses. Cancer Cell. 2025. https://doi.org/10.1016/j.ccell.2025.09.003.
12. Cervantes-Villagrana RD, Albores-García D, Cervantes-Villagrana AR, García-Acevez SJ. Tumor-induced neurogenesis and immune evasion as targets of innovative anti-cancer therapies. Signal Transduct Target Ther. 2020;5(1):99. https://doi.org/10.1038/s41392-020-0205-z.
13. Zhang Y, Guo Y, Liu Z, Sun Y, Yang X, Chen M, et al. Cancer cells co-opt an inter-organ neuroimmune circuit to escape immune surveillance. Cell. 2025. . https://doi.org/10.1016/j.cell.2025.09.029.
14. Pittet MJ, Di Pilato M, Garris C, Mempel TR. Dendritic cells as shepherds of T cell immunity in cancer. Immunity. 2023;56(10):2218–30. https://doi.org/10.1016/j.immuni.2023.08.014.
15. Tchekneva EE, Goruganthu MUL, Uzhachenko RV, Thomas PL, Antonucci A, Chekneva I, et al. Determinant roles of dendritic cell-expressed Notch Delta-like and Jagged ligands on anti-tumor T cell immunity. J Immunother Cancer. 2019;7(1):95. https://doi.org/10.1186/s40425-019-0566-4.
16. Cao J, Kong F-H, Liu X, Wang X-B. Immunotherapy with dendritic cells and cytokine-induced killer cells for hepatocellular carcinoma: A meta-analysis. World J Gastroenterol. 2019;25(27):3649–63. https://doi.org/10.3748/wjg.v25.i27.3649.

17. Zhang Q, He Y, Luo N, Patel SJ, Han Y, Gao R, et al. Landscape and dynamics of single immune cells in hepatocellular carcinoma. Cell. 2019. https://doi.org/10.1016/j.cell.2019.10.003.
18. Shang N, Figini M, Shangguan J, Wang B, Sun C, Pan L, et al. Dendritic cells based immunotherapy. Am J Cancer Res. 2017;7(10):2091–102.
19. Vivian J, Rao AA, Nothaft FA, Ketchum C, Armstrong J, Novak A, et al. Toil enables reproducible, open source, big biomedical data analyses. Nat Biotechnol. 2017;35(4):314–6. https://doi.org/10.1038/nbt.3772.
20. Dong Q, Guo Y, Lv C, Ren L, Chen B, Wang Y, et al. Unveiling a novel cancer hallmark by evaluation of neural infiltration in cancer. Brief Bioinform. 2025. https://doi.org/10.1093/bib/bbaf082.
21. Xu S, Hu E, Cai Y, Xie Z, Luo X, Zhan L, et al. Using clusterProfiler to characterize multiomics data. Nat Protoc. 2024;19(11):3292–320. https://doi.org/10.1038/s41596-024-01020-z.
22. Badia-I-Mompel P, Wessels L, Müller-Dott S, Trimbour R, Ramirez Flores RO, Argelaguet R, Saez-Rodriguez J. Gene regulatory network inference in the era of single-cell multi-omics. Nat Rev Genet. 2023;24(11):739–54. https://doi.org/10.1038/s41576-023-00618-5.
23. Azizi E, Carr AJ, Plitas G, Cornish AE, Konopacki C, Prabhakaran S, et al. Single-cell map of diverse immune phenotypes in the breast tumor microenvironment. Cell. 2018;174(5):1293–e30836. https://doi.org/10.1016/j.cell.2018.05.060.
24. Zhang Z, Wu Y, Fu J, Yu X, Su Y, Jia S, et al. Proteostatic reactivation of the developmental transcription factor TBX3 drives BRAF/MAPK-mediated tumorigenesis. Nat Commun. 2024;15(1):4108. https://doi.org/10.1038/s41467-024-48173-9.
25. Zhou J, Tison K, Zhou H, Bai L, Acharyya RK, McEachern D, et al. STAT5 and STAT3 balance shapes dendritic cell function and tumour immunity. Nature. 2025;643(8071):519–28. https://doi.org/10.1038/s41586-025-09000-3.
26. Li R, Wei K, Sun Q, Xie B, Wei P, Xie T, et al. Analysis of the three-dimensional genome of exhausted CD8 + T cells reveals a critical role of IRF8 in their differentiation and functions in cancer. Nat Immunol. 2025;26(12):2280–95. https://doi.org/10.1038/s41590-025-02330-4.
27. Williams AF, Gervasio DAG, Turkal CE, Stuhlfire AE, Wang MX, Mauch BE, et al. DNA fragmentation factor B suppresses interferon to enable cancer persister cell regrowth. Nat Cell Biol. 2025. https://doi.org/10.1038/s41556-025-01810-x.
28. Sun R, Lei C, Xu Z, Gu X, Huang L, Chen L, et al. Neutral ceramidase regulates breast cancer progression by metabolic programming of TREM2-associated macrophages. Nat Commun. 2024;15(1):966. https://doi.org/10.1038/s41467-024-45084-7.
29. Jiang M-J, Cui H-P, Li T-T, Yang X-M, Lu X-L, Liu A-Q. A novel anti-CTLA-4 nanobody-IL12 fusion protein in combination with a dendritic cell/tumour fusion cell vaccine enhances the antitumour activity of CD8 + T cells in solid tumours. J Nanobiotechnol. 2024;22(1):645. https://doi.org/10.1186/s12951-024-02914-6.
30. Moon CY, Belabed M, Park MD, Mattiuz R, Puleston D, Merad M. Dendritic cell maturation in cancer. Nat Rev Cancer. 2025;25(4):225–48. https://doi.org/10.1038/s41568-024-00787-3.
31. Ma T, Chu X, Wang J, Li X, Zhang Y, Tong D, et al. Pan-Cancer Analyses Refine the Single-Cell Portrait of Tumor-Infiltrating Dendritic Cells. Cancer Res. 2025;85(19):3596–613. https://doi.org/10.1158/0008-5472.CAN-24-3595.
32. Castenmiller C, Keumatio-Doungtsop B-C, van Ree R, de Jong EC, van Kooyk Y. Tolerogenic Immunotherapy: Targeting DC Surface Receptors to Induce Antigen-Specific Tolerance. Front Immunol. 2021;12:643240. https://doi.org/10.3389/fimmu.2021.643240.
33. Zhu S, Yang N, Wu J, Wang X, Wang W, Liu Y-J, Chen J. Tumor microenvironment-related dendritic cell deficiency: a target to enhance tumor immunotherapy. Pharmacol Res. 2020;159:104980. https://doi.org/10.1016/j.phrs.2020.104980.

Publisher's Note